





Article

Muntingia calabura Leaves Mediated Green Synthesis of CuO Nanorods: Exploiting Phytochemicals for Unique Morphology

Vidhya Selvanathan ¹, Mohammad Aminuzzaman ^{2,3,*}, Lai-Hock Tey ², Syaza Amira Razali ¹, Khaled Althubeiti ⁴, Hend Ibraheem Alkhamash ⁵, Samar Kumar Guha ⁶, Sayaka Ogawa ⁷, Akira Watanabe ⁷, Md. Shahiduzzaman ⁸ and Md. Akhtaruzzaman ^{1,*}

- ¹ Solar Energy Research Institute (SERI), Universiti Kebangsaan Malaysia (UKM), Bangi 43600, Malaysia; vidhya@ukm.edu.my (V.S.); mirarazali@gmail.com (S.A.R.)
- ² Department of Chemical Science, Faculty of Science, Universiti Tunku Abdul Rahman (UTAR), Perak Campus, Jalan Universiti, Bandar Barat, Kampar 31900, Malaysia; teylh@utar.edu.my
- ³ Centre for Photonics and Advanced Materials Research (CPAMR), Universiti Tunku Abdul Rahman (UTAR), Jalan Sungai Long, Bandar Sungai Long, Kajang 43000, Malaysia
- ⁴ Department of Chemistry, College of Science, Taif University, P.O. Box 11099, Taif 21944, Saudi Arabia; k.althubeiti@tu.edu.sa
- ⁵ Department of Electrical Engineering, College of Engineering, Taif University, Taif 21944, Saudi Arabia; Khamash.h@tu.edu.sa
- ⁶ Department of Arts and Sciences, Faculty of Engineering, Ahsanullah University of Science and Technology, 141-142, Love Road, Tejgaon I/A, Dhaka 1208, Bangladesh; skguha.as@aust.edu
- ⁷ Institute of Multidisciplinary Research for Advanced Materials (IMRAM), Tohoku University, Sendai 980-8577, Japan; sayaka.ogawa.a1@tohoku.ac.jp (S.O.); akira.watanabe.c6@tohoku.ac.jp (A.W.)
- ⁸ Nanomaterials Research Institute (NanoMaRi), Kanazawa University, Kakuma, Kanazawa 920-1192, Japan; shahiduzzaman@se.kanazawa-u.ac.jp
- * Correspondence: mohammoda@utar.edu.my (M.A.); akhtar@ukm.edu.my (M.A.)



Citation: Selvanathan, V.; Aminuzzaman, M.; Tey, L.-H.; Razali, S.A.; Althubeiti, K.; Alkhamash, H.I.; Guha, S.K.; Ogawa, S.; Watanabe, A.; Shahiduzzaman, M.; et al. *Muntingia calabura* Leaves Mediated Green Synthesis of CuO Nanorods: Exploiting Phytochemicals for Unique Morphology. *Materials* **2021**, *14*, 6379. <https://doi.org/10.3390/ma14216379>

Academic Editor: Claudio Evangelisti

Received: 21 August 2021

Accepted: 11 October 2021

Published: 25 October 2021

Publisher's Note: MDPI stays neutral with regard to jurisdictional claims in published maps and institutional affiliations.



Copyright: © 2021 by the authors. Licensee MDPI, Basel, Switzerland. This article is an open access article distributed under the terms and conditions of the Creative Commons Attribution (CC BY) license (<https://creativecommons.org/licenses/by/4.0/>).

Abstract: In this study, phytochemical assisted nanoparticle synthesis was performed using *Muntingia calabura* leaf extracts to produce copper oxide nanoparticles (CuO NPs) with interesting morphology. Scanning electron microscope (SEM) and transmission electron microscope (TEM) analysis of the biosynthesized CuO NPs reveal formation of distinct, homogeneous, and uniform sized CuO nanorods structure with thickness and length of around 23 nm and 79 nm, respectively. Based on Fourier-transform infrared (FTIR) analysis, the unique combinations of secondary metabolites such as flavonoid and polyphenols in the plant extract are deduced to be effective capping agents to produce nanoparticles with unique morphologies similar to conventional chemical synthesis. X-ray diffraction (XRD) analysis verified the monoclinical, crystalline structure of the CuO NPs. The phase purity and chemical identity of the product was consolidated via X-Ray photoelectron spectroscopy (XPS) and Raman spectroscopic data which indicate the formation of a single phase CuO without the presence of other impurities. The direct and indirect optical band gap energies of the CuO nanorods were recorded to be 3.65 eV and 1.42 eV.

Keywords: copper oxide; nanorods; green synthesis; *Muntingia calabura*

1. Introduction

Copper oxide nanoparticles (NPs) are the multifunctional members of the family of copper compounds, with unique properties compared to its macroscopic counterparts. Copper oxide in the stoichiometric form of CuO, also known as cupric oxide, is a p-type semiconductor with band gap of 1.7 eV. Due to their high surface area to volume ratio, CuO NPs are widely used in sensors, energy storage devices, antimicrobial activity, environmental remediation, and catalytic applications [1–4]. To date, several experimental methods have been utilized to synthesize CuO NPs, including sol-gel process [5], electrochemical approach [6], sonochemistry [7], and microwave irradiation [8]. While the conventional

wet chemistry method was very effective in producing homogeneously sized CuO NPs, the environmental hazards posed by the usage of certain chemical species remained a major concern [9,10]. This dilemma paved the way for novel attempts to synthesize CuO NPs using plant extracts as the more sustainable method [11–13]. The biosynthesis of different metal oxide nanostructures including nickel oxide [14], cobalt oxide [15], iron oxide [16], and zinc oxide [17] have been reported using various parts of different plant species [18]. To date, a variety of phytochemicals containing plant extracts such as *Cordia sebestena* flower [19], *Rheum palmatum* L. root [20], *Euphorbia pulcherrima* flower [21], and *Caesalpinia bonducella* seed [22] have been reported for successful synthesis of CuO NPs.

While the structural integrity and elemental purity of such green-synthesized CuO NPs have been on par with those synthesized via traditional chemical methods, the morphological properties of the nanomaterial still have room for improvement [23]. In contrast to interesting morphologies, including nanorods, nanowires, nanosheets, and nanoflowers that are reported for chemically synthesized CuO NPs [24,25], green synthesis most often yields spherical or quasi-spherical nanoparticles that are agglomerated into a cluster. This might restrict the application of green synthesized CuO NPs as particle size and shape of nanoparticles govern their physicochemical properties, which in turn dictates their functionality. For instance, Ajibade et al. compared the photocatalytic properties of platinum disulfide nanoparticles in different morphologies such as bead-shape, quasi-spherical and spherical [26]. It was evident that the shape of the nanoparticles affected effective surface area, porosity, and band gap of the material which in turn influenced its efficiency in photocatalytic degradation of dye molecules. In this regard, the choice of plant extract used during the synthesis process plays a crucial role in the mechanism of ion reduction, capping, and stabilization of CuO NPs, ultimately influencing the morphology of the nanostructure.

Hence, in this study, we have attempted to use *Muntingia calabura* leaf extracts for the synthesis of CuO nanorods. *M. calabura* is synonymously known as “Jamaican cherry” throughout the world, and in Malaysia it is usually cultivated as roadside trees [27]. The leaves of this tropical plant species have been traditionally used as tranquillizer, headache remedy, and tonic in several cultures. Recent studies, aimed to determine the bioactive compounds in *M. calabura*, reveal that the leaves are rich in glycosides, tannins, flavonoids, and terpenoids [28–31]. This unique cocktail of phytochemicals in the *M. calabura* leaves extract are exploited as an ideal medium for synthesis of CuO NPs with unique morphology.

2. Materials and Methods

2.1. Materials

Fresh *Muntingia calabura* leaves were collected from roadside trees in Kampar, Malaysia. Copper (II) nitrate trihydrate [Cu(NO₃)₂·3H₂O] was purchased from Quality Reagent Chemical, QRëC, New Zealand, and used as purchased.

2.2. Preparation of Plant Extract

Freshly plucked *M. calabura* leaves were washed with tap water and allowed to air dry at room temperature for 5 days. Once dried, the leaves were ground to fine powder. In the preliminary step, CuO NPs were synthesized by using different amounts (0.5 g, 1 g, 2 g, and 5 g) of *M. calabura* leaves powder suspended in 100 mL deionized water, followed by heating at 80 °C for 20 min [32–34]. However, the best formation of nanoparticles was achieved with the concentration of 2 g of *M. calabura* leaves in 100 mL water. The light brown solution was then filtered to remove solid particles and stored in a refrigerator.

2.3. Green Synthesis of CuO Nanoparticles

For the synthesis of CuO NPs, 50 mL solution of 0.5 M copper (II) nitrate trihydrate was prepared. We added 10 mL of the *M. calabura* leaves extract dropwise to the copper precursor solution and the mixture was stirred at 80 °C for 4 h. This resulted in a greenish paste which was allowed to cool to room temperature. The paste was calcined at 400 °C

for 2 h, producing fine, black CuO powder. Figure 1 summarizes the synthesis of natural extract mediated CuO NPs.

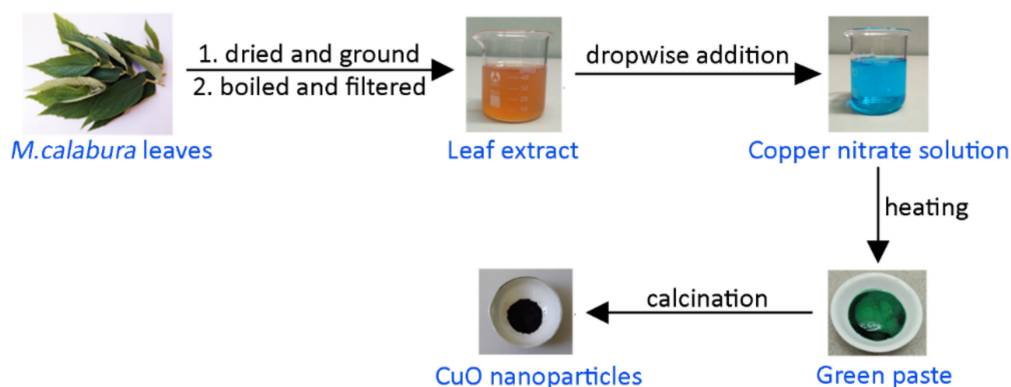


Figure 1. Experimental procedure for green synthesis of CuO nanoparticles.

2.4. Characterization of CuO Nanoparticles

The crystal properties of the sample were characterized from 10 to 80° in 2θ by an X-ray diffractometer with $\text{CuK}\alpha$ radiation (Shimadzu XRD 6000, Kyoto, Japan). Morphological characteristics were characterized by FESEM (JEOL JSM-6701F combined with EDX, Tokyo, Japan) and high resolution transmission electron microscope (HRTEM) (JEOL JEM 3010). UV–Vis absorption spectra were recorded by a UV–visible spectrophotometer (Perkin Elmer Lambda 35, (Waltham, MA, USA)). The FTIR spectra of biosynthesized CuO NPs were recorded by KBr pellet method using FTIR spectrophotometer (Perkin Elmer RX1). The X-ray photoelectron spectra were obtained using Perkin Elmer PHI5600 (ULVAC-PHI, Inc., Waltham, MA, USA). A micro-Raman spectrometer equipped with an optical microscope (Olympus BX51, Tokyo, Japan), a CW 532 nm DPSS laser, a Peltier-cooled CCD camera (DV401, Andor Technology, Belfast, UK) and a monochromator (MS257, Oriel Instruments Co., Stratford, CT, USA) were used to measure the Raman spectra.

3. Results and Discussions

3.1. Structural Analysis

The X-ray diffractogram of *M. calabura* mediated CuO nanoparticles depict sharp, intense peaks, which verifies the crystalline nature of the nanostructures. As shown in Figure 2, major diffraction peaks were evident at 2θ values of 32.51°, 36.32°, 39.20°, 49.42°, and 62.26° which are attributed to (0 3 1), (0 0 2), (1 1 1), (2 0 -2), and (1 1 -3) planes, respectively. Additionally, the minor peaks detected at 58.87°, 66.90°, 68.70°, 73.05°, and 75.68° can be assigned to the crystal planes of (2 0 2), (3 1 -1), (1 1 3), (3 1 1), and (0 0 4), respectively. The peaks detected in this study coincide with previously reported literature on CuO NPs [35–37] and is in agreement with International Centre for Diffraction Data (ICDD): Entry number-00-045-0937. Based on the XRD peak positions, it can be concluded that the CuO NPs synthesized via the phytochemical method has a monoclinic phase with lattice parameters of $a = 4.6853 \text{ \AA}$, $b = 3.4257 \text{ \AA}$, $c = 5.1303 \text{ \AA}$, and $\beta = 99.549 \text{ \AA}$. The distinct, well-defined XRD peaks without any impurity peaks is a further testament to the purity of CuO NPs obtained using the reported method.

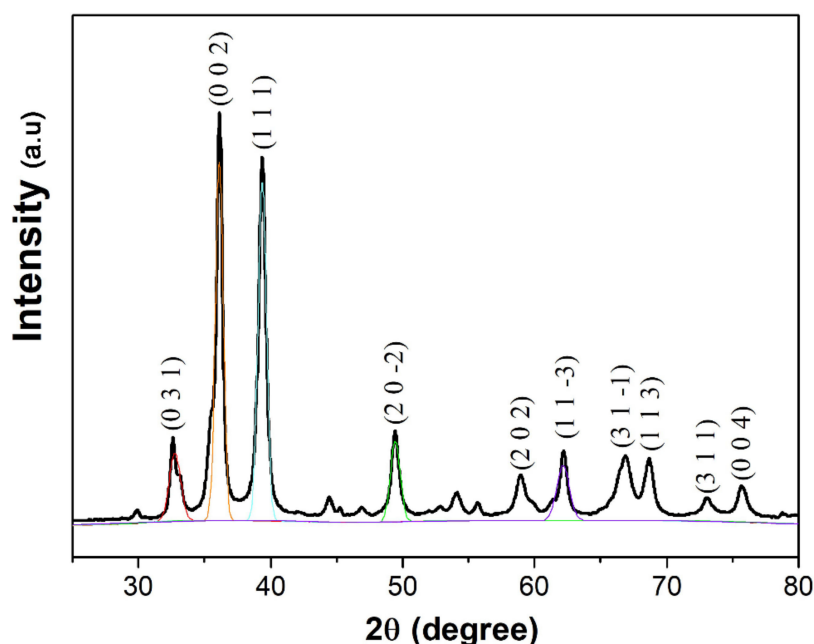


Figure 2. X-ray diffractogram of *M. calabura* derived CuO nanoparticles.

To gain an insight on the average crystallite size (D) of the CuO NPs, the XRD peaks were analysed using the Debye-Scherrer equation, which states:

$$D = \frac{k\lambda}{\beta \cos\theta}, \quad (1)$$

where k is the shape constant (taken to be 0.9), λ is the wavelength of the X-ray radiation (in nm), β is the full width half maximum of the peak (in radians), and θ is the diffraction angle (in degrees). Table 1 shows the average crystallite size based on the prominent XRD peaks which ranges between 12 to 20 nm. It is crucial to note that the crystallite size of non-spherical structures calculated using this method may have deviations due to the effect of shape factor value used in Debye-Scherrer's formula. Besides that, occurrence of non-single crystal, heterogeneous crystal strain, and instrumental effects may also deviate the calculated value from actual ones.

Table 1. Particle size distribution based on Debye-Scherrer's equation.

2θ	Miller Index	FWHM ($^\circ$)	β (Radians)	D (nm)
32.51	(0 3 1)	0.71	0.0124	11.65
36.32	(0 0 2)	0.41	0.0072	20.38
39.20	(1 1 1)	0.57	0.0099	14.80
49.42	(2 0 -2)	0.63	0.0110	13.88
62.26	(1 1 -3)	0.75	0.0131	12.36

The monoclinic CuO nanocrystal structure and phase purity were further validated based on the Raman spectrum of the product as shown in Figure 3. As the space group of CuO is C_{2h}^6 , the zone centre Raman active normal modes of CuO are $\Gamma_{RA} = 4A_u + 5B_u + A_g + 2B_g$. Between these vibration modes, there are three Raman active modes, namely one A_g and two B_g [38]. The Raman spectrum of the CuO NPs clearly shows peaks at 288, 324, and 621 cm^{-1} , which corresponds to the typical modes of A_g and two B_g , respectively. The wavenumbers detected in this study are found to be at lower values compared to Raman spectra of CuO nanostructures prepared by microwave irradiation method in previous literature (296, 346, and 631 cm^{-1}) [38]. This could be an impact of smaller grain size of the CuO NPs, which is reported to shift the Raman bands to smaller wavenumbers [39].

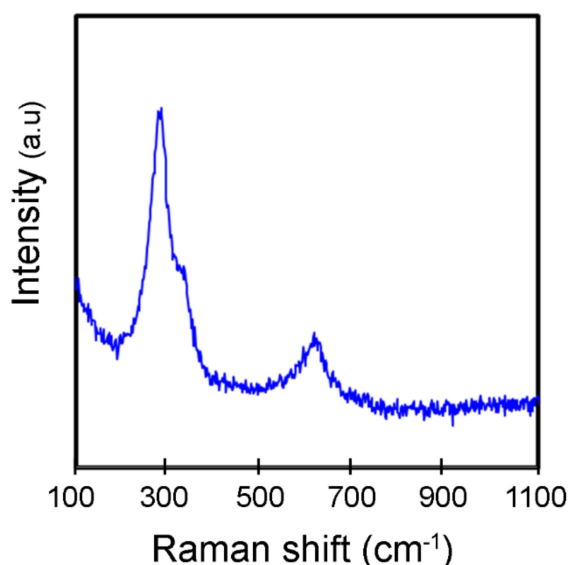


Figure 3. Raman spectrum of *M. calabura* derived CuO nanoparticles.

To comprehend the chemical composition of the green synthesized CuO NPs, the sample was subjected to XPS analysis and the survey scan of XPS spectrum depicts major peaks corresponding to C 1s, O 1s, and Cu 2p (Figure 4a). Figure 4b depicts the high resolution Cu 2p spectrum with binding energies of 931.6 and 951.4 eV that are indicative of Cu 2p_{3/2} and Cu 2p_{1/2}, respectively, which correspond to Cu²⁺ state of valency. The gap between both the peaks is around 20 eV, which coincides with standard CuO XPS spectrum. The Cu 2p_{3/2} shakeup satellite peak appears at about 941.5 eV and the satellite peak of Cu 2p_{1/2} lies at about 961.5 eV. Both these values are consistent with other CuO NPs systems [40,41]. The occurrence of shakeup satellite structures for Cu 2p spectrum eliminates the possibility of any Cu₂O phase present in the product. The O 1s spectrum (Figure 4c) of particles exhibit the binding energy allocated at 529.46 eV which corresponds to O 1s of Cu-O bonding. In addition, the Gaussian fitting between 526–536 eV region resolves another peak at 531.32 eV that is attributed to presence of surface adsorbed oxygen. Overall, the XPS analysis of green synthesized CuO NPs confirms that the product is in a single phase without presence of other impurities.

3.2. Optical Analysis

The UV–Vis absorption spectrum of the CuO NPs was analysed by forming a 0.1 wt% dispersion of the product using deionized water. The UV–Vis absorption spectrum (Figure 5a) illustrates a rather broad absorption which peaks at 387 nm and is most probably attributed to surface plasmon resonance (SPR) due to semiconductor excitation of CuO [42]. Using the Tauc plot approach, the band gap energy (E_g) of the CuO NPs was derived with the following equation:

$$\alpha h\nu = A(h\nu - E_g)^n, \quad (2)$$

where h is incident photon energy, n is the exponent factor that governs the electronic transition ($n = 1/2$ for direct band and $n = 2$ for indirect band), and α is the absorption coefficient. Figure 5b depicts the extrapolation of the Tauc plot with the direct optical band gap energy of the CuO NPs attaining 3.65 eV. The direct band gap recorded in this study is similar to CuO nanoellipsoids synthesized by Boltaev et al. using the laser ablation method [43]. The higher bandgap of the synthesized nanorods compared to bulk CuO is attributed to the quantum size effect. When particle size approaches the nanoscale dimension, the overlapping of adjacent energy levels minimizes and subsequently the width of energy band widens [44]. As the optical properties of the CuO nanorods also

indicate the presence of indirect band gap, the Tauc plot derivative for indirect optical bandgap calculation is depicted in Figure 5c. The nanorods show an indirect band gap of 1.42 eV, which coincides with the reported literature value for monoclinic cupric oxide structure [45].

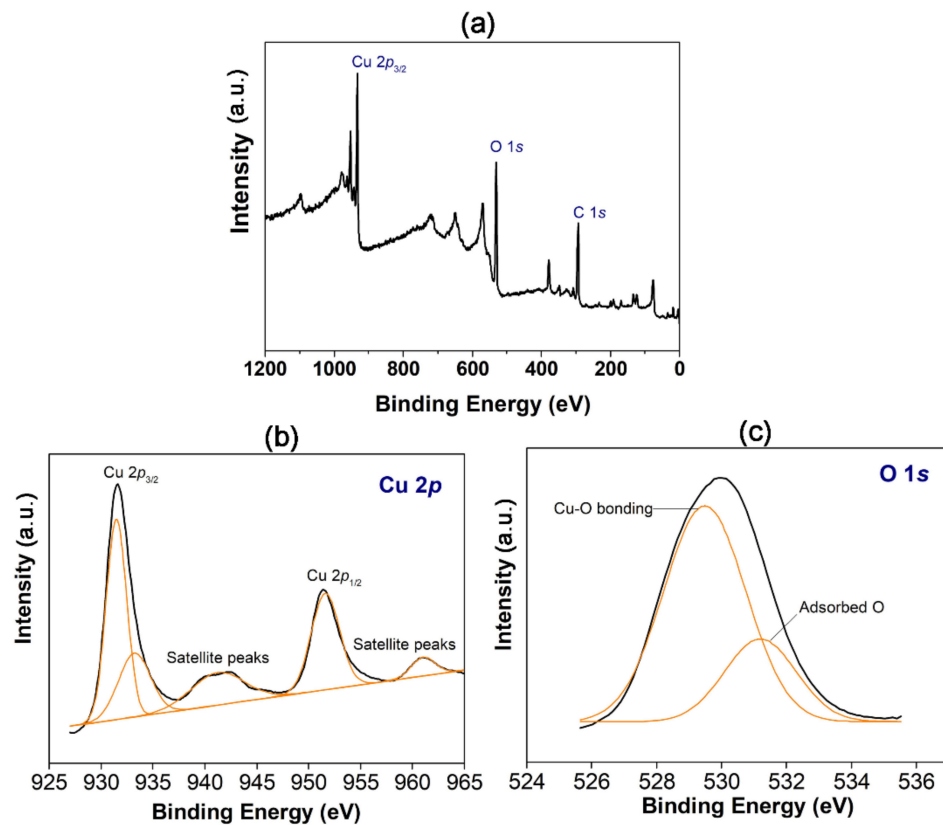


Figure 4. (a) XPS survey spectra of *M. calabura* derived CuO nanoparticles, (b) high-resolution Cu 2p peaks, and (c) high-resolution O 1s peaks.

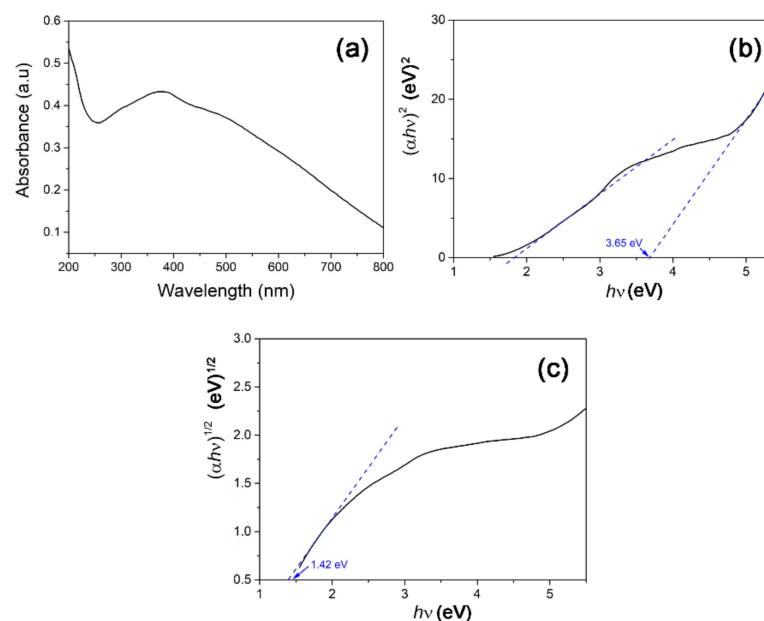


Figure 5. (a) UV-Vis absorption spectrum of *M. calabura* derived CuO nanoparticles and the corresponding Tauc plot for (b) direct and (c) indirect band gap.

3.3. Morphological Analysis

The structural properties of CuO NPs were investigated using FESEM analysis, as shown in Figure 6a. The nanoparticles seemingly displayed a rod-like morphology with uniformity in terms of size and particle distribution. In fact, the nanorods appear as distinct structures without much agglomeration, as opposed to agglomerated clusters often observed in most phytochemical assisted CuO NP synthesis. Figure 6b shows the elemental compositions of the sample gauged using EDX analysis, which reveal copper and oxygen as the sole elements present.

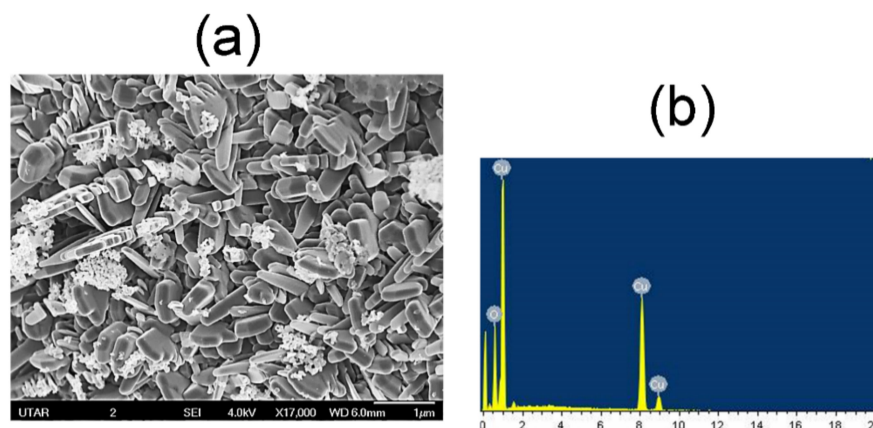


Figure 6. (a) FESEM images and (b) EDX spectrum of *M. calabura* derived CuO nanoparticles.

To elucidate the nanoparticle size and morphology, TEM analysis was performed. Figure 7 shows that the green synthesized CuO nanostructures are clearly in rod shape with thickness around 23 nm and length between 79 to 90 nm. The particle size demonstrated in morphological analysis was bigger than the crystallite size estimated from XRD analysis, hence indicating that the single CuO particle is composed of few crystallites. Table 2 compares the morphological properties of previously reported CuO NP synthesis using phytochemicals. It is evident that the nanoparticle morphology obtained in this study is novel compared to the other systems, and this is an effect of the unique combinations of biomolecules present in the *M. calabura* leaves extract. Particularly, synthesis of CuO nanorods is usually achieved via addition of strong bases, chemical surfactants, or capping agents. In this work, the CuO nanorods can be achieved by simply using the *M. calabura* leaves extract in place of these chemicals. In fact, no organic solvent is used for extraction of phytochemicals from the plant. It is interesting to note that a similar nanostructure can be obtained by employing a green extract, allowing the synthesis process to be cheaper and more sustainable.

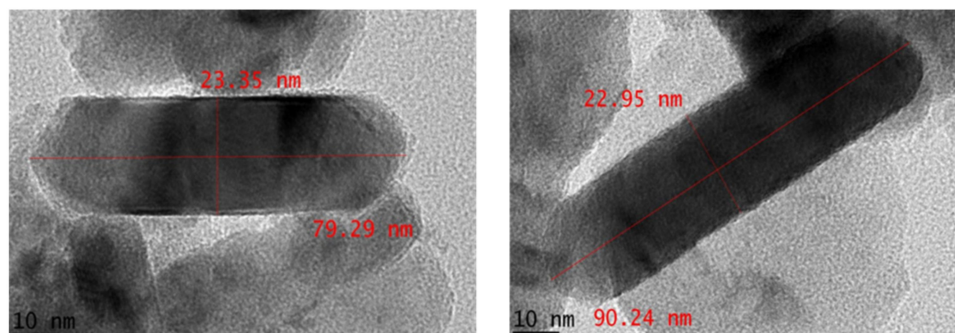


Figure 7. TEM images of *M. calabura* derived CuO nanoparticles.

Table 2. Comparison of morphological properties of CuO NPs derived from *M. calabura* leaves with recent literature.

Source of Phytochemical	Smallest Particle Size (nm)	Shape	References
<i>Madhuca longifolia</i> seeds	30	Quasi-spherical	[46]
<i>Carica papaya</i> peel	85	Irregular	[47]
<i>Anthemis nobilis</i> flowers	61	Irregular	[48]
<i>Musa acuminata</i> peel	50	Spherical	[49]
<i>Psidium guajava</i> leaves	33	Spherical	[50]
<i>Caesalpinia bonducella</i> seed	13	Rice shaped	[22]
<i>Muntingia calabura</i> leaves	23	Rod shaped	This work

3.4. Phytochemical Constituents

The *M. calabura* leaves extract was characterized using FTIR analysis to explore the presence of active groups in the plant extract that facilitates the formation of CuO nanorods. Figure 8a shows the FTIR spectrum of the *M. calabura* extract with prominent absorption bands at 3413 cm^{-1} and 1630 cm^{-1} , corresponding to the O-H bond of the polyphenols and C=O stretch of the flavonoids. The bands at 1414 cm^{-1} and 1034 cm^{-1} originate from -COO carboxylic acid and C-N amine stretch, respectively [19]. Absorption bands due to the carbohydrate components in the leaves extract are visible between 1000 to 1100 cm^{-1} . The functional group identities of the *M. calabura* extract indicates the presence of useful secondary metabolites such as glycosides, tannins, flavonoids, and terpenoids, as reported in earlier studies. The traces of these biological compounds are detectable in the FTIR spectrum of the green synthesized CuO NPs (Figure 8b). In particular, the strong absorption bands at 3428 cm^{-1} and 1640 cm^{-1} in the nanostructures indicate that the phenolic group and flavonoids served as encapsulating and stabilizing agents during the formation of CuO nanoparticles [51]. The intense peak at 452 cm^{-1} is recognized to be the characteristic peaks of CuO. Previously, Senthilkumar et al. studied a possible mechanism for the synthesis of ZnO NPs using *Tectona grandis* L. leaf extract [52]. They suggested that phenols and flavonoids in the aqueous leaf extract bind the surface of zinc in precursor to activate the formation of nanoparticles. The FTIR analysis of CuO NPs in this case show comparable results to their observation.

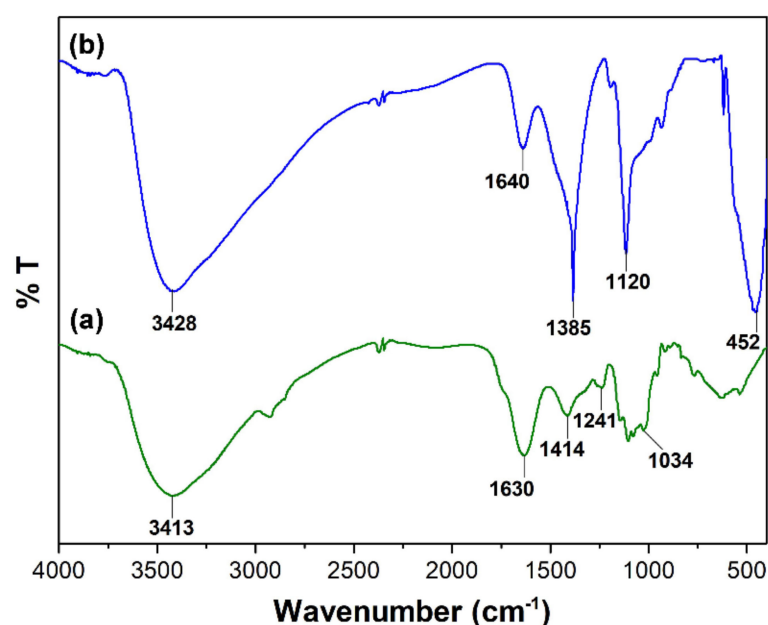
**Figure 8.** FTIR spectra of (a) *M. calabura* extract and (b) CuO nanoparticles.

Figure 9 illustrates the possible mechanisms adapted for the formation of CuO nanorods with the aid of biomolecules in *M. calabura* extract. To date, two different approaches have been suggested in the literature to comprehend the plausible mechanism route of the biosynthesis of metal oxide nanoparticles using phytochemicals. In the first approach, the active ingredients in the plant extract, such as flavonoids and phenols, chelate with the precursor copper ions to form coordinated complexes [17]. These intermediate complexes would then thermally degrade upon calcination and form copper oxide nanorods. Several studies reported earlier supports the chelation theory for formation of metal oxide nanoparticles [53,54]. For instance, Matinise et al. (2017) proposed that the antioxidants in *Moringa oleifera* leaves chelate with the zinc (II) ions, leading to formation of zinc complexes, which is later converted to zinc oxide nanoparticles after heat treatment [55]. They further corroborated this mechanism by observing FTIR absorption bands characteristic to the bioactive compounds in the plant extract being present in the green synthesized zinc oxide nanoparticles. Alternatively, Singh et al. proposed a bioreduction mechanism for the green synthesis of zinc oxide quantum dots using the mixture of *Eclipta alba* leaf extract and zinc acetate [56]. In this mechanism, the first step involves the reduction in metal ions to zero-valent states using the bioreducing agents present in the plant extract. The reduced metal atoms are then converted to ZnO as a result of the reaction with the dissolved oxygen (O_2) content in the reaction mixture. A similar mechanism has been suggested in several other studies, adopting green synthesis of metal oxide nanoparticles [57,58]. Interestingly, in the bioreduction mechanism, it is also proposed that the phytochemicals in the extract also aid particle stabilization by hindering agglomeration of the formed nanoparticles.

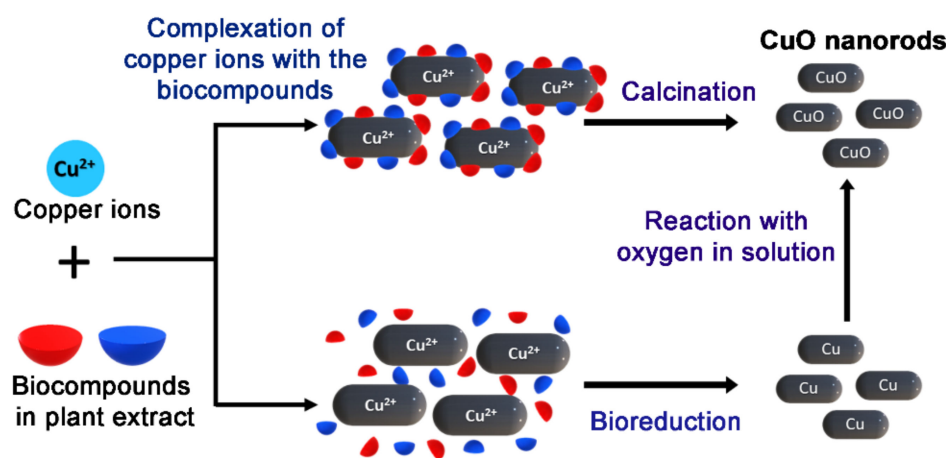


Figure 9. Possible reaction mechanism for *M. calabura* mediated CuO nanoparticles synthesis.

4. Conclusions

The potential application of *M. calabura* leaf extracts as reducing and capping agents for the synthesis of copper oxide nanoparticles (CuO NPs) is explored for the first time. The green synthesis method was successful in producing highly crystalline, pure CuO nanostructures as confirmed by the presence of characteristic peaks in an XRD analysis. Based on XPS and Raman spectrum, the single phase properties and structural integrity of the product were verified. In contrast to the typical spherical nanoparticle clusters observed in previously reported green synthesized CuO NPs, morphological properties of the product in this study depict the formation of well defined, non-agglomerated CuO nanorods with an average thickness of 23 nm and length between 79 to 90 nm. Based on FTIR analysis, it is deduced that the presence of secondary metabolites, particularly flavonoids and phenols in the *M. calabura* leaf extracts, play an important role in directing and stabilizing the unique rod-like morphology of the CuO NPs.

Author Contributions: Conceptualization, M.A. (Mohammad Aminuzzaman) and M.A. (Md. Akhtaruzzaman); methodology, L.-H.T. and S.A.R.; formal analysis, S.A.R.; resources, M.S., K.A., H.I.A. and S.K.G.; data curation, V.S., S.O. and A.W. and L.-H.T.; writing—V.S.; writing—review and editing, V.S., S.O. and A.W.; supervision, M.A. (Md. Akhtaruzzaman) and M.A. (Mohammad Aminuzzaman); and funding acquisition, S.K.G., M.S., K.A. and H.I.A. All authors have read and agreed to the published version of the manuscript.

Funding: The authors are highly grateful to Universiti Kebangsaan Malaysia for supporting this study through the Modal Insan fellowship (RFA1). Authors also extended their appreciation to The University Researchers Supporting Project Number (TURSP-2020/241), Taif University, Taif, Saudi Arabia.

Institutional Review Board Statement: Not applicable.

Informed Consent Statement: Not applicable.

Data Availability Statement: The data presented in this study are available upon request from the corresponding author.

Acknowledgments: The authors are highly grateful to Universiti Kebangsaan Malaysia for supporting this study through the Modal Insan fellowship (RFA1). Authors also extended their appreciation to The University Researchers Supporting Project Number (TURSP-2020/241), Taif University, Taif, Saudi Arabia. Authors are thankful to Universiti Tunku Abdul Rahman (UTAR) for financial support and also providing all necessary research facilities to carry out this research work successfully.

Conflicts of Interest: The authors declare no conflict of interest.

References

1. Rabiee, N.; Bagherzadeh, M.; Kiani, M.; Ghadiri, A.M.; Etesamifar, F.; Jaberizadeh, A.H.; Shakeri, A. Biosynthesis of copper oxide nanoparticles with potential biomedical applications. *Int. J. Nanomed.* **2020**, *15*, 3983–3999. [\[CrossRef\]](#)
2. Alizadeh, T.; Mirzagholipur, S. A Nafion-free non-enzymatic amperometric glucose sensor based on copper oxide nanoparticles–graphene nanocomposite. *Sens. Actuators B Chem.* **2014**, *198*, 438–447. [\[CrossRef\]](#)
3. Rajkumar, S.; Elanthamilan, E.; Balaji, T.E.; Sathiyar, A.; Jafneel, N.E.; Merlin, J.P. Recovery of copper oxide nanoparticles from waste SIM cards for supercapacitor electrode material. *J. Alloys Compd.* **2020**, *849*, 156582. [\[CrossRef\]](#)
4. Singh, J.; Kumar, V.; Kim, K.-H.; Rawat, M. Biogenic synthesis of copper oxide nanoparticles using plant extract and its prodigious potential for photocatalytic degradation of dyes. *Environ. Res.* **2019**, *177*, 108569. [\[CrossRef\]](#) [\[PubMed\]](#)
5. Wu, H.-Q.; Wei, X.-W.; Shao, M.-W.; Gu, J.-S.; Qu, M.-Z. Synthesis of copper oxide nanoparticles using carbon nanotubes as templates. *Chem. Phys. Lett.* **2002**, *364*, 152–156. [\[CrossRef\]](#)
6. Shashanka, R.; Swamy, B.E.K. Simultaneous electro-generation and electro-deposition of copper oxide nanoparticles on glassy carbon electrode and its sensor application. *SN Appl. Sci.* **2020**, *2*, 956. [\[CrossRef\]](#)
7. Silva, N.; Ramírez, S.; Díaz, I.; Garcia, A.; Hassan, N. Easy, quick, and reproducible sonochemical synthesis of CuO nanoparticles. *Materials* **2019**, *12*, 804. [\[CrossRef\]](#)
8. Ponnar, M.; Thangamani, C.; Monisha, P.; Gomathi, S.S.; Pushpanathan, K. Influence of Ce doping on CuO nanoparticles synthesized by microwave irradiation method. *Appl. Surf. Sci.* **2018**, *449*, 132–143. [\[CrossRef\]](#)
9. Tobiszewski, M.; Namieśnik, J.; Pena-Pereira, F. Environmental risk-based ranking of solvents using the combination of a multimedia model and multi-criteria decision analysis. *Green Chem.* **2017**, *19*, 1034–1042. [\[CrossRef\]](#)
10. Bleam, W.F. Chapter 7—Acid-Base Chemistry. In *Soil and Environmental Chemistry*; Bleam, W.F., Ed.; Academic Press: Boston, MA, USA, 2012; pp. 257–319. [\[CrossRef\]](#)
11. Hassan, H.M.A.; Alhumaimess, M.S.; Alsohaimi, I.H.; Essawy, A.A.; Hussein, M.F.; Alshammari, H.M.; Aldosari, O.F. Biogenic-mediated synthesis of the Cs₂O–MgO/MPC nanocomposite for biodiesel production from olive oil. *ACS Omega* **2020**, *5*, 27811–27822. [\[CrossRef\]](#)
12. Alhumaimess, M.S.; Essawy, A.A.; Kamel, M.M.; Alsohaimi, I.H.; Hassan, H.M.A. Biogenic-mediated synthesis of mesoporous Cu₂O/CuO nano-architectures of superior catalytic reductive towards nitroaromatics. *Nanomaterials* **2020**, *10*, 781. [\[CrossRef\]](#)
13. Essawy, A.A.; Alsohaimi, I.H.; Alhumaimess, M.S.; Hassan, H.M.A.; Kamel, M.M. Green synthesis of spongy nano-ZnO productive of hydroxyl radicals for unconventional solar-driven photocatalytic remediation of antibiotic enriched wastewater. *J. Environ. Manag.* **2020**, *271*, 110961. [\[CrossRef\]](#)
14. Gebretinsae, H.G.; Tsegay, M.G.; Nuru, Z.Y. Biosynthesis of nickel oxide (NiO) nanoparticles from cactus plant extract. *Mater. Today Proc.* **2021**, *36*, 566–570. [\[CrossRef\]](#)
15. Dubey, S.; Kumar, J.; Kumar, A.; Sharma, Y.C. Facile and green synthesis of highly dispersed cobalt oxide (Co₃O₄) nano powder: Characterization and screening of its eco-toxicity. *Adv. Powder Technol.* **2018**, *29*, 2583–2590. [\[CrossRef\]](#)
16. Martínez-Cabanás, M.; López-García, M.; Barriada, J.L.; Herrero, R.; Sastre de Vicente, M.E. Green synthesis of iron oxide nanoparticles. Development of magnetic hybrid materials for efficient As(V) removal. *Chem. Eng. J.* **2016**, *301*, 83–91. [\[CrossRef\]](#)

17. Bandeira, M.; Giovanela, M.; Roesch-Ely, M.; Devine, D.M.; da Silva Crespo, J. Green synthesis of zinc oxide nanoparticles: A review of the synthesis methodology and mechanism of formation. *Sustain. Chem. Pharm.* **2020**, *15*, 100223. [[CrossRef](#)]
18. Rana, A.; Yadav, K.; Jagadevan, S. A comprehensive review on green synthesis of nature-inspired metal nanoparticles: Mechanism, application and toxicity. *J. Clean. Prod.* **2020**, *272*, 122880. [[CrossRef](#)]
19. Prakash, S.; Elavarasan, N.; Venkatesan, A.; Subashini, K.; Sowndharya, M.; Sujatha, V. Green synthesis of copper oxide nanoparticles and its effective applications in *Biginelli* reaction, BTB photodegradation and antibacterial activity. *Adv. Powder Technol.* **2018**, *29*, 3315–3326. [[CrossRef](#)]
20. Bordbar, M.; Sharifi-Zarchi, Z.; Khodadadi, B. Green synthesis of copper oxide nanoparticles/clinoptilolite using *Rheum palmatum* L. root extract: High catalytic activity for reduction of 4-nitro phenol, rhodamine B, and methylene blue. *J. Sol-Gel Sci. Technol.* **2017**, *81*, 724–733. [[CrossRef](#)]
21. Sackey, J.; Nwanya, A.C.; Bashir, A.K.H.; Matinise, N.; Ngilirabanga, J.B.; Ameh, A.E.; Coetsee, E.; Maaza, M. Electrochemical properties of *Euphorbia pulcherrima* mediated copper oxide nanoparticles. *Mater. Chem. Phys.* **2020**, *244*, 122714. [[CrossRef](#)]
22. Sukumar, S.; Rudrasenan, A.; Padmanabhan Nambiar, D. Green-synthesized rice-shaped copper oxide nanoparticles using *Caesalpinia bonducella* seed extract and their applications. *ACS Omega* **2020**, *5*, 1040–1051. [[CrossRef](#)]
23. Siddiqi, K.S.; Husen, A. Current status of plant metabolite-based fabrication of copper/copper oxide nanoparticles and their applications: A review. *Biomater. Res.* **2020**, *24*, 11. [[CrossRef](#)] [[PubMed](#)]
24. Sun, S.; Zhang, X.; Sun, Y.; Yang, S.; Song, X.; Yang, Z. Hierarchical CuO nanoflowers: Water-required synthesis and their application in a nonenzymatic glucose biosensor. *Phys. Chem. Chem. Phys.* **2013**, *15*, 10904–10913. [[CrossRef](#)] [[PubMed](#)]
25. Singh, B.K.; Shaikh, A.; Dusane, R.O.; Parida, S. Copper oxide nanosheets and nanowires grown by one-step linear sweep voltammetry for supercapacitor application. *J. Energy Storage* **2020**, *31*, 101631. [[CrossRef](#)]
26. Ajibade, P.A.; Oluwalana, A.E.; Andrew, F.P. Morphological studies, photocatalytic activity, and electrochemistry of platinum disulfide nanoparticles from bis(morpholinyl-4-carbodithioato)-platinum(II). *ACS Omega* **2020**, *5*, 27142–27153. [[CrossRef](#)]
27. Mahmood, N.D.; Nasir, N.L.M.; Rofiee, M.S.; Tohid, S.F.M.; Ching, S.M.; Teh, L.K.; Salleh, M.Z.; Zakaria, Z.A. *Muntingia calabura*: A review of its traditional uses, chemical properties, and pharmacological observations. *Pharm. Biol.* **2014**, *52*, 1598–1623. [[CrossRef](#)]
28. Sibi, G.; Naveen, R.; Dhananjaya, K.; Ravikumar, K.R.; Mallesha, H. Potential use of *Muntingia calabura* L. extracts against human and plant pathogens. *Pharmacogn. J.* **2012**, *4*, 44–47. [[CrossRef](#)]
29. Buhian, W.P.C.; Rubio, R.O.; Valle, D.L.; Martin-Puzon, J.J. Bioactive metabolite profiles and antimicrobial activity of ethanolic extracts from *Muntingia calabura* L. leaves and stems. *Asian Pac. J. Trop. Biomed.* **2016**, *6*, 682–685. [[CrossRef](#)]
30. Ragasa, C.; Tan, M.; Chiong, I.; Shen, C.-C. Chemical constituents of *Muntingia calabura*. *Der Pharma Chem.* **2015**, *7*, 136–141.
31. Sufian, A.S.; Ramasamy, K.; Ahmat, N.; Zakaria, Z.A.; Yusof, M.I.M. Isolation and identification of antibacterial and cytotoxic compounds from the leaves of *Muntingia calabura* L. *J. Ethnopharmacol.* **2013**, *146*, 198–204. [[CrossRef](#)]
32. Banerjee, P.; Satapathy, M.; Mukhopahayay, A.; Das, P. Leaf extract mediated green synthesis of silver nanoparticles from widely available Indian plants: Synthesis, characterization, antimicrobial property and toxicity analysis. *Bioresour. Bioprocess.* **2014**, *1*, 3. [[CrossRef](#)]
33. Karuppiah, M.; Rajmohan, R. Green synthesis of silver nanoparticles using *Ixora coccinea* leaves extract. *Mater. Lett.* **2013**, *97*, 141–143. [[CrossRef](#)]
34. El-Borady, O.M.; Ayat, M.S.; Shabrawy, M.A.; Millet, P. Green synthesis of gold nanoparticles using Parsley leaves extract and their applications as an alternative catalytic, antioxidant, anticancer, and antibacterial agents. *Adv. Powder Technol.* **2020**, *31*, 4390–4400. [[CrossRef](#)]
35. Saravanakumar, K.; Shanmugam, S.; Varukattu, N.B.; MubarakAli, D.; Kathiresan, K.; Wang, M.-H. Biosynthesis and characterization of copper oxide nanoparticles from indigenous fungi and its effect of photothermolysis on human lung carcinoma. *J. Photochem. Photobiol. B Biol.* **2019**, *190*, 103–109. [[CrossRef](#)]
36. Phiw dang, K.; Suphankij, S.; Mekprasart, W.; Pecharapa, W. Synthesis of CuO nanoparticles by precipitation method using different precursors. *Energy Procedia* **2013**, *34*, 740–745. [[CrossRef](#)]
37. Muthuvel, A.; Jothibas, M.; Manoharan, C. Synthesis of copper oxide nanoparticles by chemical and biogenic methods: Photocatalytic degradation and in vitro antioxidant activity. *Nanotechnol. Environ. Eng.* **2020**, *5*, 14. [[CrossRef](#)]
38. Tran, T.H.; Nguyen, V.T. Copper oxide nanomaterials prepared by solution methods, some properties, and potential applications: A brief review. *Int. Sch. Res. Not.* **2014**, *2014*, 856592. [[CrossRef](#)]
39. Rashad, M.; Rüsing, M.; Berth, G.; Lischka, K.; Pawlis, A. CuO and Co₃O₄ nanoparticles: Synthesis, characterizations, and raman spectroscopy. *J. Nanomater.* **2013**, *2013*, 714853. [[CrossRef](#)]
40. Song, Y.; Cho, D.; Venkateswarlu, S.; Yoon, M. Systematic study on preparation of copper nanoparticle embedded porous carbon by carbonization of metal–organic framework for enzymatic glucose sensor. *RSC Adv.* **2017**, *7*, 10592–10600. [[CrossRef](#)]
41. Sudha, V.; Murugadoss, G.; Thangamuthu, R. Structural and morphological tuning of Cu-based metal oxide nanoparticles by a facile chemical method and highly electrochemical sensing of sulphite. *Sci. Rep.* **2021**, *11*, 3413. [[CrossRef](#)]
42. Thamer, N.A.; Muftin, N.Q.; Al-Rubae'i, S.H.N. Optimization properties and characterization of green synthesis of copper oxide nanoparticles using aqueous extract of *Cordia myxa* L. leaves. *Asian J. Chem.* **2018**, *30*, 1559–1563. [[CrossRef](#)]
43. Boltaev, G.S.; Ganeev, R.A.; Krishnendu, P.S.; Zhang, K.; Guo, C. Nonlinear optical characterization of copper oxide nanoellipsoids. *Sci. Rep.* **2019**, *9*, 11414. [[CrossRef](#)]

44. Talluri, B.; Prasad, E.; Thomas, T. Ultra-small ($r < 2$ nm), stable (>1 year) copper oxide quantum dots with wide band gap. *Superlattices Microstruct.* **2018**, *113*, 600–607. [[CrossRef](#)]
45. Dhineshababu, N.R.; Rajendran, V.; Nithyavathy, N.; Vetumperumal, R. Study of structural and optical properties of cupric oxide nanoparticles. *Appl. Nanosci.* **2016**, *6*, 933–939. [[CrossRef](#)]
46. Sankar, R.; Manikandan, P.; Malarvizhi, V.; Fathima, T.; Shivashangari, K.S.; Ravikumar, V. Green synthesis of colloidal copper oxide nanoparticles using *Carica papaya* and its application in photocatalytic dye degradation. *Spectrochim. Acta Part A Mol. Biomol. Spectrosc.* **2014**, *121*, 746–750. [[CrossRef](#)]
47. Phang, Y.-K.; Aminuzzaman, M.; Akhtaruzzaman, M.; Muhammad, G.; Ogawa, S.; Watanabe, A.; Tey, L.-H. Green synthesis and characterization of CuO nanoparticles derived from papaya peel extract for the photocatalytic degradation of palm oil mill effluent (POME). *Sustainability* **2021**, *13*, 796. [[CrossRef](#)]
48. Nasrollahzadeh, M.; Sajadi, S.M.; Rostami-Vartooni, A. Green synthesis of CuO nanoparticles by aqueous extract of *Anthemis nobilis* flowers and their catalytic activity for the A3 coupling reaction. *J. Colloid Interface Sci.* **2015**, *459*, 183–188. [[CrossRef](#)]
49. Aminuzzaman, M.; Kei, L.M.; Liang, W.H. Green synthesis of copper oxide (CuO) nanoparticles using banana peel extract and their photocatalytic activities. *AIP Conf. Proc.* **2017**, *1828*, 020016. [[CrossRef](#)]
50. Sreeju, N.; Rufus, A.; Philip, D. Studies on catalytic degradation of organic pollutants and anti-bacterial property using biosynthesized CuO nanostructures. *J. Mol. Liq.* **2017**, *242*, 690–700. [[CrossRef](#)]
51. Król, A.; Railean-Plugaru, V.; Pomastowski, P.; Buszewski, B. Phytochemical investigation of *Medicago sativa* L. extract and its potential as a safe source for the synthesis of ZnO nanoparticles: The proposed mechanism of formation and antimicrobial activity. *Phytochem. Lett.* **2019**, *31*, 170–180. [[CrossRef](#)]
52. Senthilkumar, N.; Nandhakumar, E.; Priya, P.; Soni, D.; Vimalan, M.; Vetha Potheher, I. Synthesis of ZnO nanoparticles using leaf extract of *Tectona grandis* (L.) and their anti-bacterial, anti-arthritic, anti-oxidant and in vitro cytotoxicity activities. *New J. Chem.* **2017**, *41*, 10347–10356. [[CrossRef](#)]
53. Fazlzadeh, M.; Khosravi, R.; Zarei, A. Green synthesis of zinc oxide nanoparticles using *Peganum harmala* seed extract, and loaded on *Peganum harmala* seed powdered activated carbon as new adsorbent for removal of Cr(VI) from aqueous solution. *Ecol. Eng.* **2017**, *103*, 180–190. [[CrossRef](#)]
54. Nava, O.J.; Luque, P.A.; Gómez-Gutiérrez, C.M.; Vilchis-Nestor, A.R.; Castro-Beltrán, A.; Mota-González, M.L.; Olivas, A. Influence of *Camellia sinensis* extract on zinc oxide nanoparticle green synthesis. *J. Mol. Struct.* **2017**, *1134*, 121–125. [[CrossRef](#)]
55. Matinise, N.; Fuku, X.G.; Kaviyarasu, K.; Mayedwa, N.; Maaza, M. ZnO nanoparticles via *Moringa oleifera* green synthesis: Physical properties & mechanism of formation. *Appl. Surf. Sci.* **2017**, *406*, 339–347. [[CrossRef](#)]
56. Singh, A.K.; Pal, P.; Gupta, V.; Yadav, T.P.; Gupta, V.; Singh, S.P. Green synthesis, characterization and antimicrobial activity of zinc oxide quantum dots using *Eclipta alba*. *Mater. Chem. Phys.* **2018**, *203*, 40–48. [[CrossRef](#)]
57. Sutradhar, P.; Saha, M. Green synthesis of zinc oxide nanoparticles using tomato (*Lycopersicon esculentum*) extract and its photovoltaic application. *J. Exp. Nanosci.* **2016**, *11*, 314–327. [[CrossRef](#)]
58. Gupta, M.; Tomar, R.S.; Kaushik, S.; Mishra, R.K.; Sharma, D. Effective antimicrobial activity of green ZnO nano particles of *Catharanthus roseus*. *Front. Microbiol.* **2018**, *9*, 2030. [[CrossRef](#)]